Journal of Engineering Science and Technology Review 18 (2) (2025) 108- 115

Research Article

JOURNAL OF
Engineering Science and Technology Review

www.jestr.org

Numerical Simulation Analysis of Surrounding Rock Stability for Highway Tunnels Crossing Fault Zones

Qingyun Huang[1], Jinhuo Zheng[2], Shuimei Chen[1], Xu Chang[3] and Tao Luo[1,*]

[1]*School of Resource Engineering, Longyan University, Longyan 364012, China*
[2]*Fujian Provincial Institute of Architectural Design and Research Co., Ltd. Fuzhou 350001, China*
[3] *College of Civil Engineering, Huaqiao University, Xiamen 361021, China*

Received 7 January 2025; Accepted 29 March 2025

Abstract

To investigate the stability of tunnels crossing fault zones, a case study was conducted on an extra-long highway tunnel in Fujian Province of China by using the finite element method. The stability characteristics of the tunnel crossing four faults (namely F_0, F_1, F_2, and F_3, with different stratigraphic layers, scales, attitudes, and degrees of fragmentation) were analyzed. The stress in the surrounding rock, the displacement around the tunnel, and the evolution characteristics of the plastic zone in the surrounding rock were explored. Results show that, the dip angle, dip direction of the faults, the intersection between the tunnel and the faults, and the degree of fault fragmentation have substantial effects on tunnel stability. Stress in the surrounding rock is concentrated near the faults, the largest displacement occurs at the tunnel sidewalls, and the stability of the surrounding rock near the fault zones is poor. Among the four faults, F_0 and F_1 are stable and only require shotcrete and bolt support. However, there need reinforcement measures such as denser, longer bolts or steel support near F_2 and F_3 for higher stresse. Additionally, the excavation sequence and speed should be reasonably controlled to minimize stress concentration and surrounding rock damage caused by excavation. The obtained conclusions provide the theoretical support and technical reference for stability studies of tunnels crossing fault zones in tunnel engineering.

Keywords: Tunnel engineering, Stability analysis, Fault zone, Surrounding rock

1. Introduction

The stability of tunnels when crossing fault zones is a current technical difficulty in tunnel engineering [1]. In the face of complex stratigraphy and landforms, large-scale faults, variable attitudes, and varying degrees of rock mass fragmentation, effectively addressing issues such as surrounding rock deformation, stress concentration, and the stability of rock masses around faults remains a significant challenge in tunnel engineering [2, 3]. The stability of tunnels is particularly crucial when they approach large-scale faults, where the potential for instability increases due to the complex stress distributions and potential deformation in the surrounding rock. Therefore, there is a pressing need for in-depth research on how to propose reasonable design support schemes during tunnel excavation, effectively control surrounding rock deformation, and enhance the safety and stability of fault zones [4, 5].

Accurate assessment of the stability of surrounding rock under different geological conditions, especially in the vicinity of large-scale faults, is crucial for designing appropriate support schemes and ensuring tunnel safety. This requires further exploration of advanced techniques such as geological mapping, geophysical surveys, and numerical modeling to gain insights into the potential deformation and failure mechanisms of the rock mass. By understanding these mechanisms, engineers can design more effective support systems that can withstand the anticipated stresses and deformations. Moreover, during tunnel construction and operation, designing more rationalized and refined support schemes to cope with geological changes and degrees of rock mass fragmentation in fault zones is essential [6, 7]. This includes selecting appropriate materials, determining the optimal support spacing, and implementing comprehensive monitoring systems to continuously assess the stability of the tunnel. The rationalization and refinement of support schemes can improve construction quality and efficiency, while also reducing the risk of tunnel instability and potential accidents.

This study takes the engineering background of an ultra-long highway tunnel in Fujian Province of China crossing fault zones with different stratigraphic layers, scales, attitudes, and degrees of fragmentation. The numerical simulation method is used to analyze the variation characteristics of stress, displacement, and rock mass failure extent in the surrounding rock as the tunnel excavation approaches the faults. The study explores the optimization of support schemes of tunnel crossing different faults, and evaluates the stability of the surrounding rock of the tunnel by conducting real-time monitoring of stress and displacement in the tunnel's surrounding rock. This provides a basis for the support design of the tunnel engineering crossing fault zones, ensuring the safety and stability of the tunnel excavation in such areas.

2. State of the art

In recent years, numerous scholars have conducted extensive research on the displacement field, stress field evolution

*E-mail address: Luotao@lyun.edu.cn
ISSN: 1791-2377
doi:10.25103/jestr.182.13

characteristics, support, and monitoring of tunnel surrounding rock when crossing faults. Regarding the characteristics of the displacement and stress fields, Saiyar et al. [8] analyzed the development of tunnel cracks under fault displacement through centrifugal model tests. Arora et al. [9] studied the deformation and failure causes of compressive tunnels. Duan et al. [10] investigated the deformation and failure characteristics of surrounding rock in tunnels with weak rock masses. Yang et al. [11] explored the damage mechanisms of soft rock roadways in deep coal mines. However, these studies have deficiencies in comprehensively considering fault characteristics (such as dip angle, dip direction, and scale), which leads to potentially one-sided research results.

In terms of construction support, Massoud and Jafar [12] proposed that crossing fault zones can significantly affect tunnel excavation speed and even lead to shutdowns. Mehdi Abbas [13] used FLAC3D and Phase2 software to analyze reinforcement schemes for tunnels crossing fault zones, but deficiencies remain in addressing construction issues related to different fault characteristics. Rehman et al. [14] proposed the back analysis approach of rock mass quality calculation from tunnel span and installed support. Kanik and Gurocak [15] obtained the optimum support elements via comparative numerical analysis. Liu et al. [16] performed the parametric analysis to discuss the influences of the factors such as frictional angle, cohesion, overburden depth, ground surface surcharge, and slurry weight on incipient failure origination as well as support pressure.

In terms of monitoring, Lin et al. [17, 18] studied the effect of faults on tunnel stability through field monitoring, numerical simulations, and microseismic monitoring. However, issues such as inadequate coverage of monitoring networks and low monitoring frequencies in actual projects limit a comprehensive understanding of tunnel stability [19-22]. The application of information and digital technologies in the field of monitoring is key to improving the efficiency and safety of tunnel engineering.

Given the limitations and gaps in the above research, this study takes an extra-long highway tunnel in Fujian Province of China as the object and uses the finite element method to analyze the stability of the tunnel when crossing fault zones. A computational model was constructed to simulate the deformation and stress distribution of surrounding rock when the tunnel crosses four faults, namely F_0, F_1, F_2, and F_3, with different stratigraphic layers, fault scales, attitudes, and degrees of fragmentation. The stress variation characteristics of the tunnel surrounding rock were analyzed, the reasons for the maximum displacement of the sidewalls were studied, the characteristics of vault settlement were analyzed, and support schemes for crossing different faults were determined. The plastic zone and potential failure range were analyzed to reveal the influence of tunnel excavation on surrounding formations.

The rest of this study is organized as follows. Section 3 elaborates on the engineering background, model establishment, and simulation scheme. Section 4 analyzes the stress, lateral displacement, vault settlement, and potential failure range of the tunnel surrounding rock. Section 5 summarizes the conclusions.

3. Methodology

3.1 Engineering background

The overall orientation of an extra-long highway tunnel is southwest to northeast. The tunnel in Fujian Province of China is designed with two routes: left and right. The tunnel body plan consists of gentle curves and straight lines. The mileage of the left line is from LK18 + 480 to LK23 + 695, with a total tunnel length of 5215 m, a clear width of 12.5 m, and a clear height of 5.0 m. The mileage of the right line is from RK18 + 500 to RK23 + 800, with a total tunnel length of 5300 m, a clear width of 12.5 m, and a clear height of 5.0 m (Fig. 1).

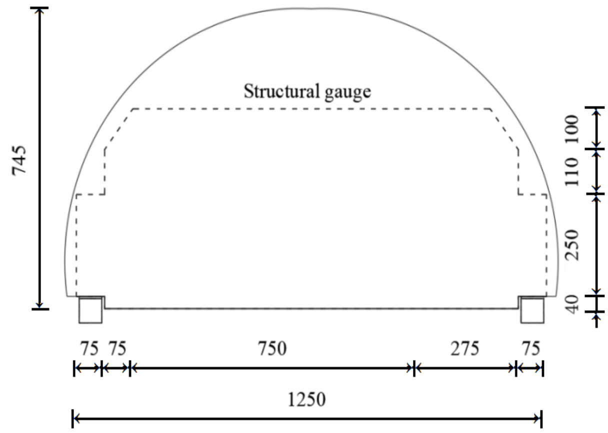

Fig. 1. Outline diagram of the tunnel section (cm)

Based on engineering geology and borehole drilling revelations, the area through which the tunnel passes consists of Jurassic rhyolite and tuffaceous rhyolite. Apart from four faults, there are no active fault structures that affect site stability. Representative faults are selected for tunnel construction simulation based on the relationship between fault strike and rock stratum strike.

(1) Fault F_0: The fault appears around mileage K18+577, with a fault plane occurrence of 225°∠75°, obliquely intersecting the tunnel route. The surrounding rock of the tunnel is relatively fragmented, and its stability is poor.

(2) Fault F_1: The tunnel obliquely intersects the fault around mileage LK19+000. Affected by this fault, the surrounding rock of the tunnel is extremely fragmented, and its stability is poor.

(3) Fault F_2: This fault dips toward SW with an angle of inclination possibly around 60°-70°. The fault strike is nearly orthogonal to the tunnel axis, directly affecting the surrounding rock of the tunnel.

(4) Fault F_3: The angle between the fault strike and the tunnel axis varies: approximately 5°-10° from K21 + 600 to K22 + 195; approximately 20° from K22 + 300 to K23 + 050; and approximately 15° from K23 + 050 to K24 + 100. The stability of the surrounding rock of the tunnel is poor.

3.2 Construction of computational models

To investigate the potential effects of fault strike and plane occurrence on tunnel excavation, numerical computational models are established for:

(1) Tunnel in the F_0 fault area: The model extends 4 times the tunnel diameter (45 m) to the left and right, and 4 times the tunnel height (30 m) downwards vertically, with an upward extension to the ground surface. The longitudinal excavation length of the tunnel model is 40m for simulation. The initial stress field of the rock mass only considers self-weight stress, excluding the influence of tectonic stress. The model is meshed using tetrahedral elements, with a total of 12,619 nodes and 44,211 elements (Fig. 2).

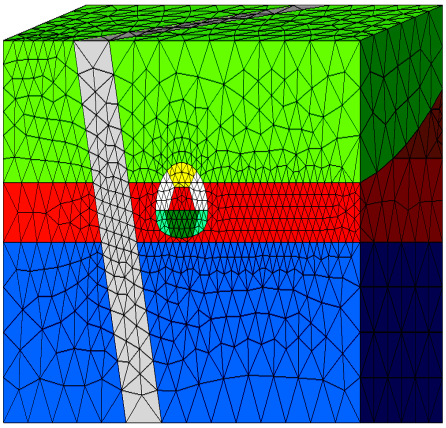

Fig. 2. Computational model for tunnel in F_0 fault area

(2) Tunnel in the F_1 fault area: The model extends 4 times the tunnel diameter (45 m) to the left and right, 4 times the tunnel height (30 m) downward vertically, and upward by 60 m (due to the relatively homogeneous lithology, a pressure load of 0.95 MPa is applied instead of modeling the stratigraphic load). The longitudinal excavation length of the tunnel is 40 m for simulation. The initial stress field of the rock mass also only considers self-weight stress. The model is meshed using tetrahedral elements, with a total of 10,261 nodes and 31,415 elements (Fig. 3)

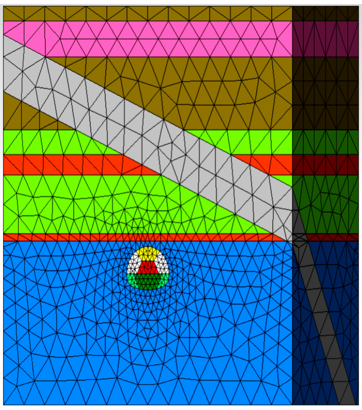

Fig. 3. Computational model for tunnel in F_1 fault area

(3) Tunnel in the F_2 fault area: The model extends 4 times the tunnel diameter (45 m) to the left and right, 4 times the tunnel height (30 m) downward vertically, and upward by 40 m (due to the relatively homogeneous lithology, a pressure load of 3 MPa is applied instead of modeling the stratigraphic load). The longitudinal excavation length of the tunnel is 40 m for simulation. The initial stress field of the rock mass only considers self-weight stress, excluding the influence of tectonic stress. The model is meshed using tetrahedral elements, with a total of 13,512 nodes and 48,931 elements (Fig. 4).

(4) Tunnel in the F_3 fault area: The model extends 4 times the tunnel diameter (45 m) to the left and right, 4 times the tunnel height (30 m) downwards vertically, and upwards by 60 m (due to the relatively homogeneous lithology, a pressure load of 4 MPa is applied instead of modeling the stratigraphic load). The longitudinal excavation length of the tunnel is 40 m for simulation. The initial stress field of the rock mass only considers self-weight stress. The model is meshed using tetrahedral elements, with a total of 11,039 nodes and 36,012 elements (Fig. 5).

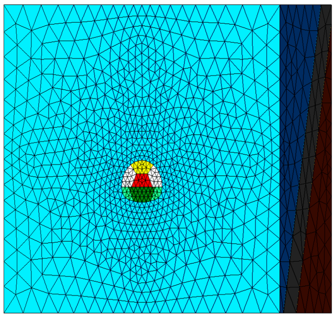

Fig. 4. Computational model for tunnel in F_2 fault area

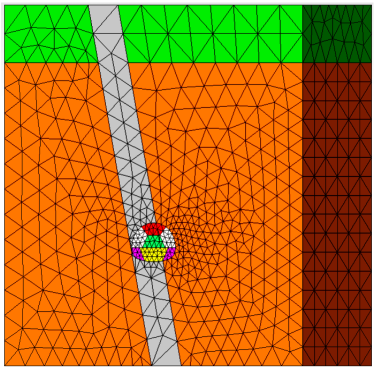

Fig. 5. Computational model for tunnel in F_3 fault area

Using the Mohr-Coulomb criterion for three-dimensional numerical simulations, the physical and mechanical parameters of the surrounding rock in the computational model tunnels are determined based on the Code for Design of Highway Tunnels (JTG 3370.1-2018) in China and previous analogous engineering analysis experience. The parameters are listed in Table 1.

Table 1. Physical and mechanical parameters of computational model

Rock mass	Elastic modulus (GPa)	Poisson's ratio	Internal friction angle (°)	Cohesion (MPa)	Density (kN/m^3)
Gravel layer	0.80	0.40	20	0.08	19.0
Tuff rock	0.90	0.40	23	0.10	22.5
Strongly weathered tuff	0.80	0.40	20	0.08	21.0
Slightly weathered rhyolite	1.50	0.35	30	0.40	22.0
Unweathered rhyolite	2.00	0.33	33	0.50	23.7
Rhyolite	2.50	0.32	35	0.60	24.0
Fault	0.50	0.45	10	0.016	16.0

3.3 Simulation analysis plan

To effectively capture the deformation, stress states, and other conditions of the surrounding rock during various stages of tunnel excavation, calculations are performed separately for the tunnel models in the four fault areas of F_0, F_1, F_2, and F_3 based on existing excavation and support methods. The analysis focuses on the characteristics of stress and displacement distributions, as well as changes in plastic zones.

The simulation of the entire tunnel excavation process utilizes the program's element (activation/deactivation) processing function, combined with the concept of equivalent release loads for tunnel excavation. The construction methods are illustrated in Fig. 6.

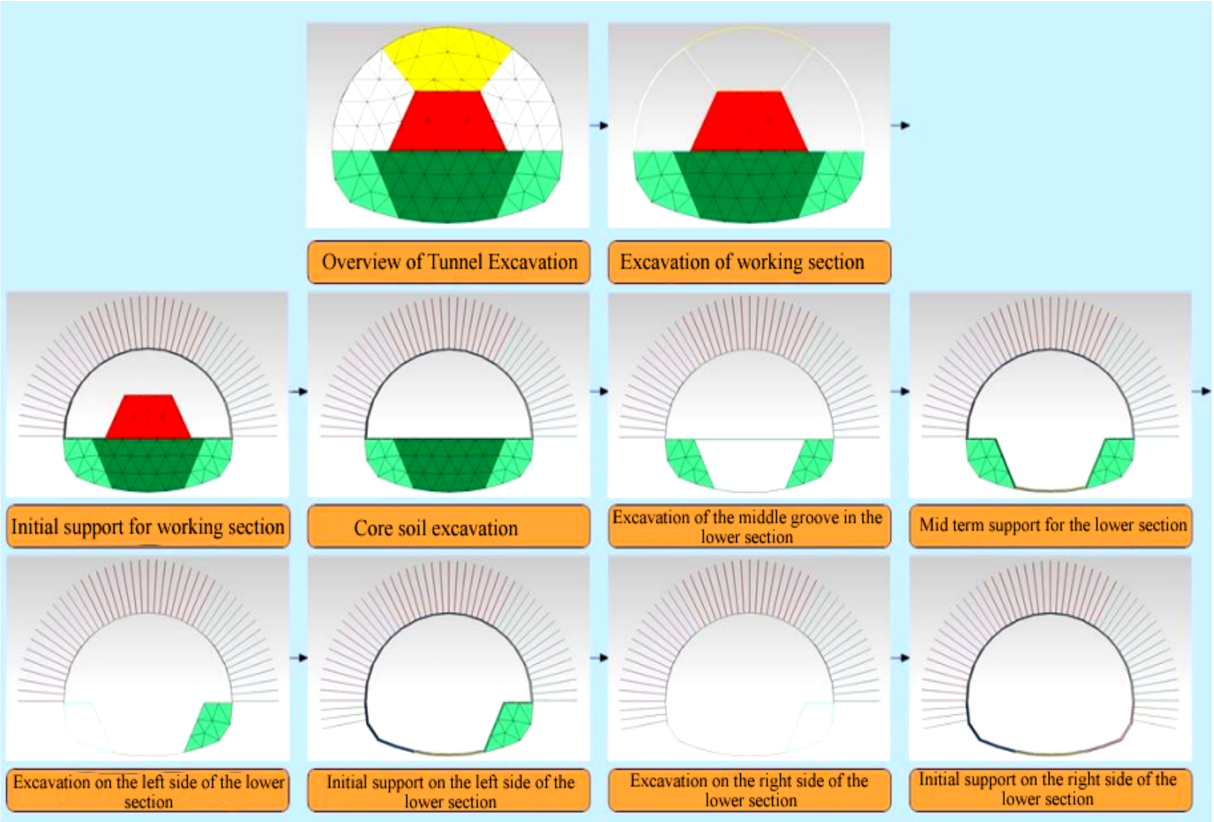

Fig. 6. Simulation diagram of construction excavation

4. Results analysis and discussion

4.1 Stress variations in tunnel surrounding rock

From Figs. 7 and 8, it can be observed that as the tunnel is excavated, the vertical stress in the lower half of the model decreases due to unloading effects, with the stress in the surrounding rock far from the tunnel entrance being relatively small. At the tunnel entrance, due to the influence of faults, there is a certain degree of stress concentration in the vertical direction [23, 24]. The maximum compressive stress occurs on the left and right side walls of the tunnel, with values of 1.13 MPa for the F_0 fault model, 6.46 MPa for the F_1 fault model, 9.73 MPa for the F_2 fault model, and 9.41 MPa for the F_3 fault model. The minimum stress is located at the tunnel crown for all models. Tensile stresses are observed at the inverted arch positions of the F_0, F_1, F_2, and F_3 tunnels. The influence of the F_3 fault results in more pronounced stress concentration within the tunnel.

When the tunnel excavation passes through the fault area, the tensile stress at the inverted arch of the F_1 tunnel decreases, while the compressive stress on the left and right side walls increases slightly. The tensile stress at the inverted arch and the compressive stress on the left and right side walls of the tunnels in fault areas F_0, F_1, F_2, and F_3 all increase to some extent. This indicates that the presence of the F_3 fault substantially enhances stress concentration within the tunnel. As the tunnel excavation approaches the fault, the secondary stress concentration resulting from tunnel excavation becomes apparent, with the maximum compressive stresses in all four fault models mainly concentrated on the left and right side walls of the tunnel.

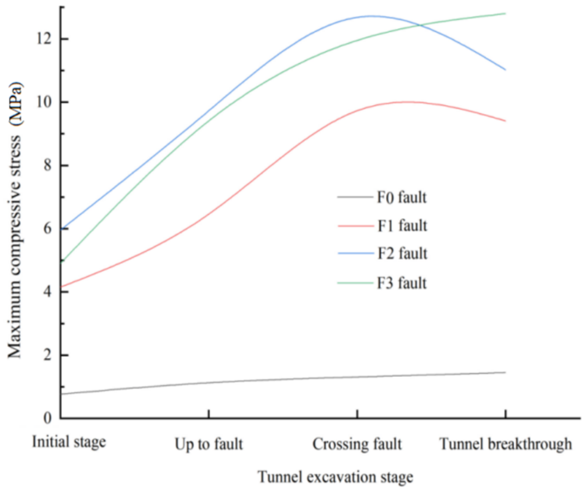

Fig. 7. Maximum vertical compressive stress of left and right sidewalls at each stage of tunnel excavation

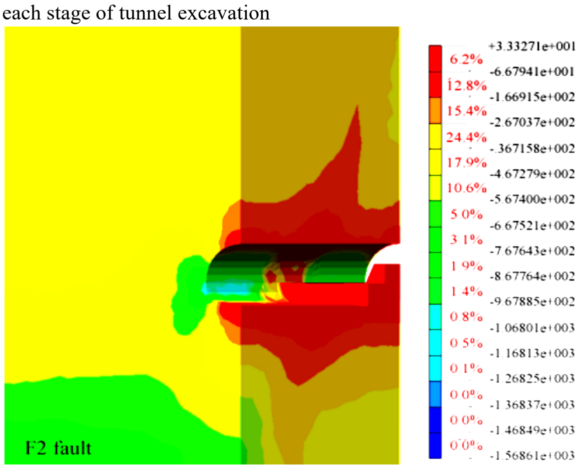

(a) F_2 fault

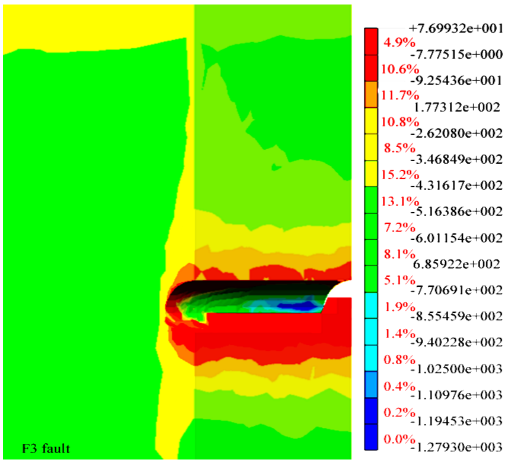

(b) F_3 fault

Fig. 8. Vertical stress distribution in fault zones during excavation (MPa)

4.2 Lateral displacement variations in the tunnel

From Figs. 9 and 10, it can be seen that when the tunnel is excavated to the locations of the four faults, the local peripheral displacement of the tunnel surrounding rock at the F_0 and F_1 faults does not show remarkable increments compared with the initial state, indicating relative safety. However, as the tunnel construction reaches the F_2 and F_3 faults, the displacement of the tunnel surrounding rock begins to increase, with sharp increases in peripheral displacement. The maximum peripheral displacement at the F_2 fault tunnel is near the tunnel waist, with a convergence value inside the tunnel suddenly increasing to 25.6 mm. The maximum peripheral displacement at the F_3 fault tunnel is near the side wall of the tunnel portal, with an outward expansion value increasing to 132.2 mm, and the affected range of tunnel surrounding rock stability increases.

The peripheral displacement of the tunnel passing through the F_0 and F_1 faults is small, indicating a relatively stable state. When passing through the F_2 fault, the maximum displacement value of the tunnel surrounding rock decreases slightly compared with before reaching the fault. The maximum displacement of the tunnel surrounding rock at the F_3 location remains near the side wall of the tunnel portal, with the outward expansion value decreasing from 132.2 mm to 60.98 mm as it approaches the fault. This is related to the influence of the fault, but it is necessary to strengthen the monitoring of the stability of the tunnel surrounding rock at the F_3 location.

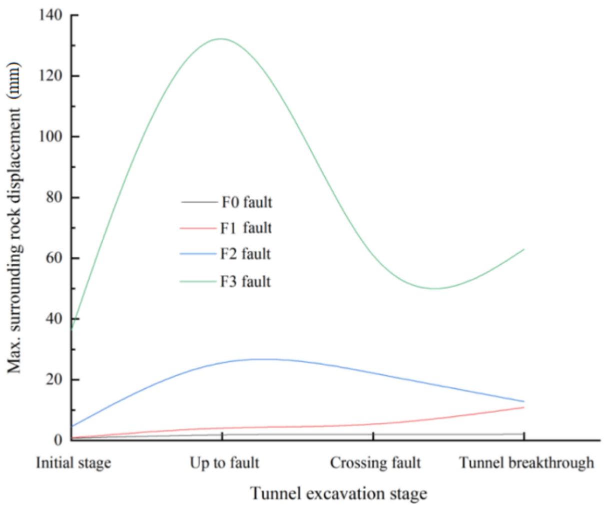

Fig. 9. Maximum displacement of surrounding rock at each stage of tunnel excavation

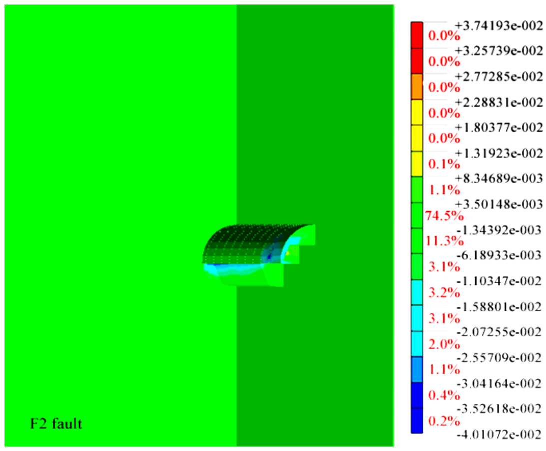

(a) F_2 fault
(b)

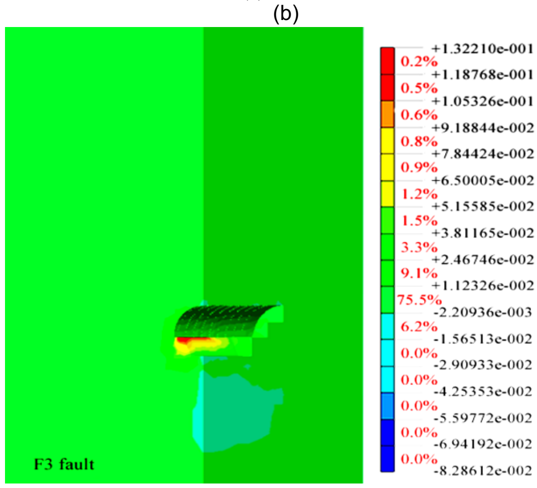

(b) F_3 fault

Fig. 10. Displacement distribution at fault zones during tunnel excavation (m)

4.3 Vault settlement analysis of tunnel surrounding rock

As seen from Figs. 11, 12, and 13, as the tunnel excavation progresses towards the faults, the stability of the surrounding rock gradually deteriorates, leading to increased vault settlement and inversion arch uplift values. At the F_0 fault, where the tunnel burial depth is relatively shallow, the tunnel settlement and inversion arch uplift values are small, with a maximum vault settlement of 3.92 mm and an inversion arch uplift value of 6.11 mm. Due to the influence of the F_1 fault, the rock mass on both sides of the valley becomes extremely fractured, causing substantial vault settlement in the tunnel surrounding rock. Simultaneously, the inversion arch uplift value is large, with a maximum vault settlement of 30.8 mm and an inversion arch uplift value sharply increasing to 179.54 mm. At the F_2 fault, the maximum vault settlement of the tunnel surrounding rock suddenly increases to 60.13 mm, with an inversion arch uplift value of 168.03 mm, representing a considerable increment compared with the initial excavation stage. The F_3 fault is affected by two NW-SE strike-slip faults, causing it to be displaced in the NW direction. This results in large vault settlement and inversion arch uplift values as tunnel excavation progresses, with a maximum vault settlement of 97.54 mm and an inversion arch uplift value as high as 317.5 mm.

When excavating the tunnel toward the faults and passing through the fault zones, the surrounding rock of the F_0 fault tunnel is in a controllable and stable state. However, at the F_1 fault, due to the presence of the fault, the surrounding rock of the tunnel is subjected to increasing stress and damage, leading to an increase in tunnel surrounding rock settlement from 30.8 mm to 38.52 mm. The inversion arch uplift value of the tunnel surrounding rock decreases from 179.54 mm to 128.6 mm. At the F_2 fault, stress release and deformation of the surrounding rock result in a decrease in tunnel surrounding rock settlement, with the inversion arch uplift value of the tunnel decreasing to 126.27 mm. At the F_3 fault, the surrounding rock of the tunnel is strongly affected by fault activity, leading to intensified deformation and damage of the surrounding rock. The settlement value is large, with the tunnel surrounding rock settlement increasing to 115.66 mm and the inversion arch uplift value decreasing to 251.35 mm.

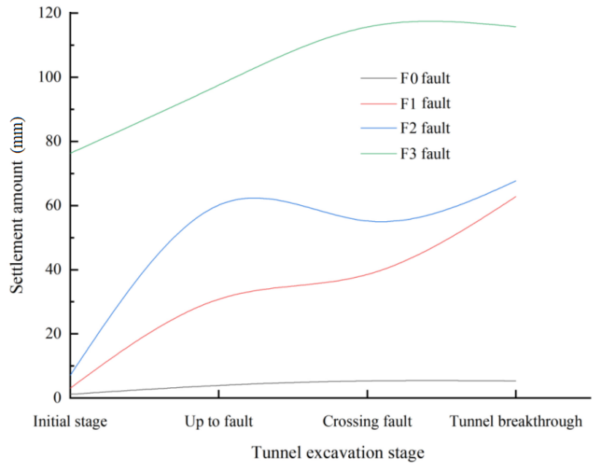

Fig. 11. Settlement of vault at each stage of tunnel excavation

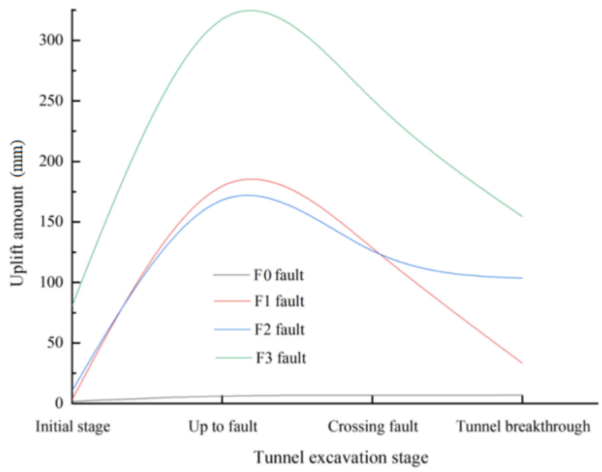

Fig. 12. Uplift amount of invert at each stage of tunnel excavation

4.4 Plastic zone and potential failure scope in tunnel

During tunnel excavation, when approaching fault locations, the plastic deformation rate of the minimum principal stress in the tunnel's main axis direction increases slightly at the F_0 fault, with a relatively small increase in magnitude and a limited plastic zone. However, at the F_1 fault, compared with the initial excavation stage, the plastic deformation rate of the tunnel surrounding rock increases substantially, reaching a maximum of 0.034. The plastic zone mainly concentrates at the tunnel face where excavation is taking place.

As excavation progresses, the plastic deformation rate at the F_2 fault location increases substantially, reaching a maximum of 0.067, with a notable increase in the plastic zone, primarily occurring at the tunnel face and the invert. So, this plastic deformation remains within a controllable range. At the F_3 fault location, the maximum plastic deformation rate of the tunnel surrounding rock reaches 0.199, indicating a significant deformation rate and an increased plastic deformation zone, primarily located at the invert. It is evident that as excavation deepens, there is a notable effect on the plastic deformation rate and zone scope.

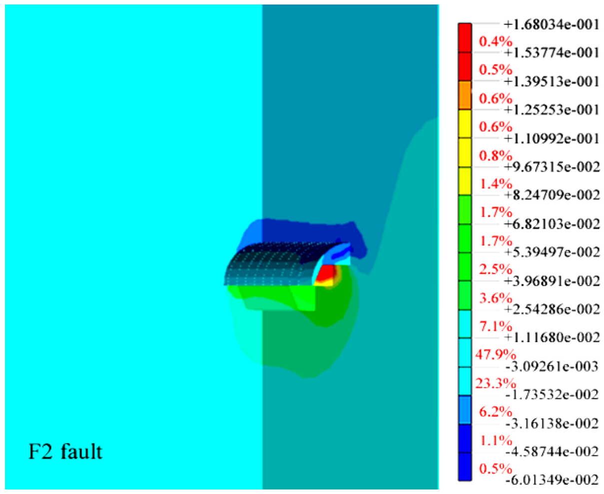

(a) F_2 fault

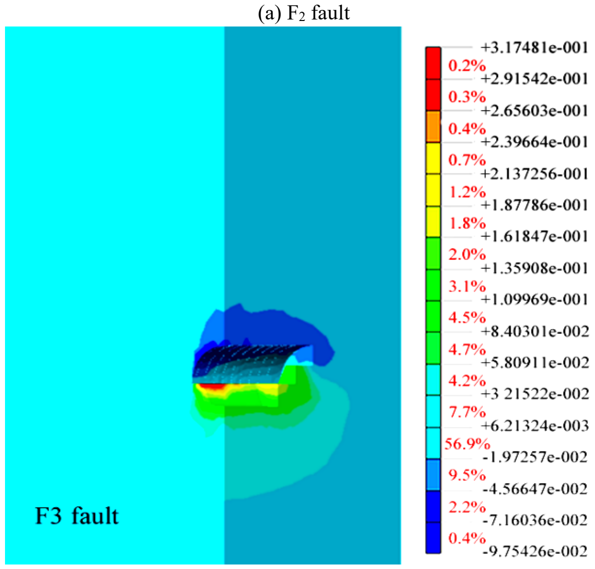

(b) F_3 fault

Fig. 13. Vault and invert deformation characteristics during excavation at fault zones (m)

When the tunnel passes through faults, the plastic deformation rate and plastic zone at the F_0 fault are small, suggesting good stability of the tunnel at this location. As the tunnel passes through the F_1 fault, the maximum plastic deformation rate of the surrounding rock is 0.039, with a small plastic zone primarily concentrated at the invert. Figs. 14 and 15 indicate that when the tunnel passes through the F_2 fault, the plastic deformation rate of the minimum principal stress in the tunnel's main axis direction is 0.058. The plastic zone of the tunnel surrounding rock decreases slightly in scope but still mainly locates at the invert, potentially affecting tunnel stability. When the tunnel passes through the F_3 fault, the plastic deformation rate of the surrounding rock reaches 0.273, with a considerable increase in the plastic zone area. The stability of the tunnel at this location is particularly crucial and requires further analysis and assessment to avoid potential instability factors and ensure the safety and stability of the tunnel.

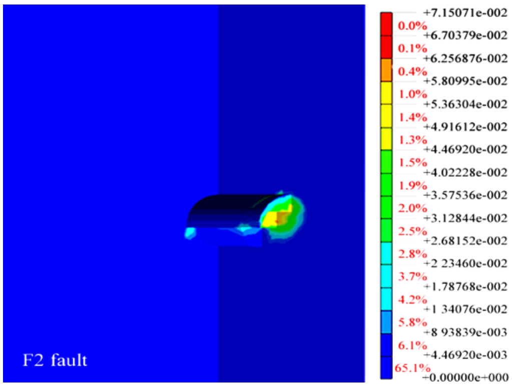

(a) F_2 fault

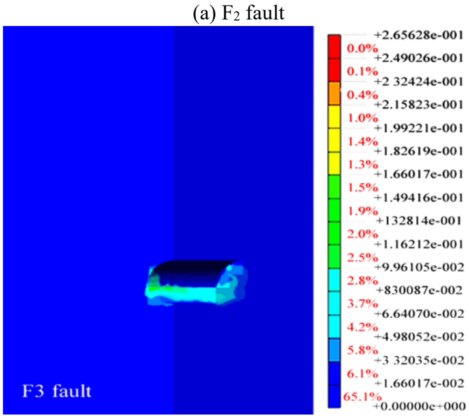

(b) F_3 fault

Fig. 14. Plastic zone distribution during excavation in fault zones

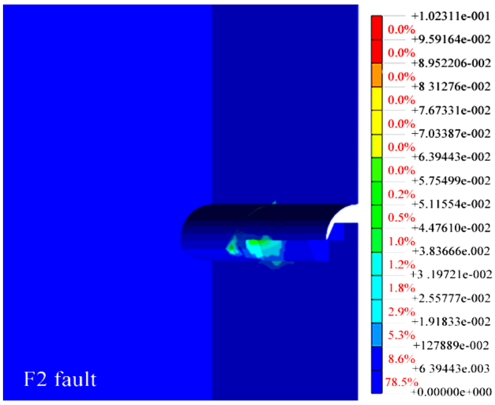

(a) F_2 fault

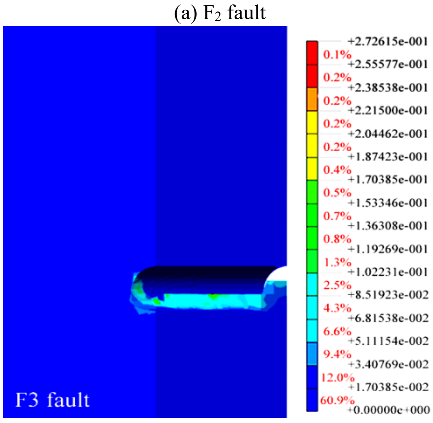

(b) F_3 fault

Fig. 15. Distribution range of plastic zone when tunnel excavates through faults

5. Conclusions

Through numerical simulation of the excavation of a super-long highway tunnel crossing four different fault zones, this study provides specific guidance for the design and construction methods of this tunnel project, effectively directing construction practices, and offers important references for the support design and construction of tunnel projects under similar geological conditions. The main conclusions drawn are as follows:

(1) Excavation in fault zones has a substantial influence on the stress and displacement states of tunnel surrounding rock. The degree of this effect is related to the characteristics of the faults (such as dip angle and dip direction), the intersection between the tunnel and the faults, and the degree of fault fragmentation. Stress concentration occurs in the tunnel surrounding rock near the four faults, with maximum displacements appearing at the left and right side walls of the tunnel. Compared with the tunnel surrounding rock far from the fault fracture zone, the stability of the tunnel surrounding rock near the fracture zone is poorer.

(2) When the tunnel excavation is close to the F_0 and F_1 faults, it is stable, and simple shotcrete and bolt support can meet the requirements. However, special attention should be paid to potential rock mass failure due to excessive stress when the tunnel excavation is close to the F_2 and F_3 faults. During tunnel construction at these two faults, reinforcement measures such as denser and longer bolts or steel supports should be adopted to reduce the disturbance and effect of the faults.

(3) By adopting a reasonable excavation sequence and speed control, the stress release and surrounding rock damage caused by tunnel excavation can be reduced. Moreover timely monitoring and tracking of tunnel surrounding rock deformation, fault activity, as well as displacement and stress changes in the tunnel's superstructure can help identify and resolve potential safety issues promptly.

Based on the occurrence and characteristics of faults and the physical and mechanical parameters of rock formations, finite element software is used to simulate the stress and displacement conditions during tunnel excavation, thereby assessing tunnel stability and providing guidance for construction. However, there are numerous factors that affect the stability of tunnel surrounding rock, and many of them cannot be accurately simulated during numerical simulation, which may result in certain errors. Therefore, the next step should involve combining actual monitoring data to adjust the design scheme in real-time, enabling numerical simulation results to be more widely applied in practical engineering.

Acknowledgements
This work was financially supported by the Natural Science Foundation of Fujian Province (2023J01959; 2022J011145), China.

References

[1] M. Zaheri, M. Ranjbarnia, and D. Dias, "3D numerical investigation of segmental tunnels performance crossing a dip-slip fault," *Geomech. Eng.*, vol. 23, no. 4, pp. 351-364, Nov. 2020.

[2] B. Bousbia, K. Goudjil, and A. Saadaoui, "Evaluation of deformations and stability of a NATM tunnel: case study Djebel El-Ouahch Tunnel, Algeria," *Studies Eng. Exact Sci.*, vol. 5, no. 2, Dec. 2024, Art. no. e11899.

[3] M. Ranjbarnia, M. Zaheri, and D. Dias, "Three-dimensional finite difference analysis of shallow sprayed concrete tunnels crossing a reverse fault or a normal fault: A parametric study," *Front. Struct. Civ. Eng.,* vol. 14, no. 4, pp. 998-1011, Jul. 2020.

[4] M. H. Baziar, A. Nabizadeh, N. Khalafian, C. J. Lee, and W. Y. Hung, "Evaluation of reverse faulting effects on the mechanical response of tunnel lining using centrifuge tests and numerical analysis," *Geotechnique*, vol. 70, no. 6, pp. 490-502, May 2020.

[5] M. Sabagh and A. Ghalandarzadeh, "Centrifuge experiments for shallow tunnels at active reverse fault intersection," *Front. Struct. Civ. Eng.*, vol. 14, no. 3, pp. 731-745, May 2020.

[6] A. G. Chermahini and H. Tahghighi, "Numerical finite element analysis of underground tunnel crossing an active reverse fault: a case study on the Sabzkouh segmental tunnel," *Geomech. Geoengin.*, vol. 14, no. 3, pp. 155-166, Feb. 2019.

[7] N. Y. Kim, D. H. Park, H. S. Jung, and M. I. Kim, "Deformation characteristics of tunnel bottom after construction under geological conditions of long-term deformation," *Geomech. Eng.*, vol. 21, no. 2, pp. 171-178, Apr. 2020.

[8] M. S. Saiyar, W. A. Take, and I. D. Moore, "Post-failure fracture angle of brittle pipes subjected to differential ground movements," *Tunn. Undergr. Sp. Tech.*, vol. 49, pp. 114-120, Jun. 2015.

[9] K. Arora, M. Gutierrez, A. Hedayat, and E. C. Cruz, "Time-Dependent Behavior of the Tunnels in Squeezing Ground: An Experimental Study," *Rock Mech. Rock Eng.*, vol. 54, no. 4, pp. 1755-1777, Feb. 2021.

[10] S. Q. Duan, X. T. Feng, Q. Jiang, G. F. Liu, S. F. Pei, and Y. L. Fan, "In situ observation of failure mechanisms controlled by rock masses with weak interlayer zones in large underground cavern excavations under high geostress," *Rock Mech. Rock Eng.*, vol. 50, no. 9, pp. 2465-2493, Jun. 2017.

[11] S. Q. Yang, M. Chen, H. W. Jing, K. F. Chen, and B. Meng, "A case study on large deformation failure mechanism of deep soft rock roadway in Xin'An coal mine, China," *Eng. Geol.*, vol. 217, no. 30, pp. 89-101, Jan. 2017.

[12] M. Bayati and J. K. Hamidi, "A case study on TBM tunnelling in fault zones and lessons learned from ground improvement," *Tunn. Undergr. Sp. Tech.*, vol. 63, pp. 162-170, Mar. 2017.

[13] M. Sabagh and A. Ghalandarzadeh, "Numerical modelings of continuous shallow tunnels subject to reverse faulting and its verification through a centrifuge," *Comput. Geotech.*, vol. 128, Dec. 2020, Art. no. 103813.

[14] H. Rehman, A. M. Naji, J. J. Kim, and H. K. Yoo, "Empirical evaluation of rock mass rating and tunneling quality index system for tunnel support design," *Appl. Sci.*, vol. 8, no. 5, May 2018, Art. no. 782.

[15] M. Kanik and Z. Gurocak, "Importance of numerical analyses for determining support systems in tunneling: A comparative study from the trabzon-gumushane tunnel, Turkey," *J. Afr. Earth Sci.*, vol. 143, pp. 253-265, Jul. 2018.

[16] W. Liu, X. Y. Zhang, B. Wu, and Y. C. Huang, "An improved mechanism for partial blowout instability of tunnel face in large slurry shield-driven tunnels," *Acta Geotech.*, vol. 19, no. 5, pp. 3021-3038, May 2024.

[17] D. Lin, R. Yuan, Y. Shang, W. Bao, K. Wang, Z. Zhang, K. Li, and W. He, "Deformation and failure of a tunnel in the restraining bend of a strike-slip fault zone: an example from Hengshan Mountain, Shanxi Province, China," *B. Eng. Geol. Environ.*, vol. 76, no. 1, pp. 263-274, Feb. 2017.

[18] Y. Wang, H. Chang, J. Wang, X. Shi, and J. Qiu, "Countermeasures to treat collapse during the construction of road tunnel in fault zone: a case study from the Yezhuping Tunnel in south Qinling, China," *Environ. Earth Sci.*, vol. 78, no. 15, Aug. 2019, Art. no. 464.

[19] Y. Wang, J. Li, Z. F. Wang, and H. Chang, "Structural failures and geohazards caused by mountain tunnel construction in fault zone and its treatment measures: A case study in Shaanxi," *Eng. Fail. Anal.*, vol. 138, Aug. 2022, Art. no. 106386.

[20] J. Shiau and S. Keawsawasvong, "Producing undrained stability factors for various tunnel shapes," *Int. J. Geomech.*, vol. 22, no. 8, Aug. 2022, Art. no. 06022017.

[21] H. Y. Lei, Y. N. Liu, Y. Hu, R. Jia, and Y. J. Zhang, "Active stability of the shield tunneling face crossing an adjacent existing tunnel: transparent clay model test and DEM simulation," *Can. Geotech. J.*, vol. 60, no. 6, pp. 864-884, Jun. 2023.

[22] Y. Su, G. F. Wang, and Q. H. Zhou, "Tunnel face stability and ground settlement in pressurized shield tunnelling," *J. Cent. South Uni.*, vol. 21, no. 4, pp. 1600-1606, Apr. 2014.

[23] J. H. Yang, S. R. Wang, Y. G. Wang, and C. L. Li, "Analysis of arching mechanism and evolution characteristics of tunnel pressure-arch," *Jordan J. Civ. Eng.*, vol. 9, no. 1, pp. 125-132, Jan. 2015.

[24] S. R. Wang, H. Q. Zhang, N. Q. Shen, and H. Y. Cao, "Analysis of deformation and stress characteristics of highway tunnels above mined-out regions," *Chin. J. Rock Mech. Eng.*, vol. 28, no. 6, pp. 1144-1151, Jun. 2009.